

Impacts of different SNLS3 light-curve fitters on cosmological consequences of interacting dark energy models

Yazhou Hu^{1,2*}, Miao Li^{3,1†}, Nan Li^{1,2‡}, Shuang Wang^{4§}

¹ State Key Laboratory of Theoretical Physics, Institute of Theoretical Physics, Chinese Academy of Sciences, Beijing 100190, P. R. China

² Kavli Institute for Theoretical Physics China, Chinese Academy of Sciences, Beijing 100190, P. R. China

³ School of Astronomy and Space Science, Sun Yat-Sen University, Guangzhou 510275, P. R. China

⁴ Department of Physics, College of Sciences, Northeastern University, Shenyang 110004, P. R. China

21 July 2022

ABSTRACT

Aims: We explore the cosmological consequences of interacting dark energy (IDE) models using the Supernova Legacy Survey three-year (SNLS3) data sets. In particular, we focus on the impacts of different SNLS3 light-curve fitters (LCF) (corresponding to the “SALT2”, the “SiFTO”, and the “Combined” supernova sample).

Methods: Firstly, making use of the three SNLS3 data sets, as well as the observational data from the cosmic microwave background (CMB), the galaxy clustering (GC) and the direct measurement of Hubble constant H_0 , we constrain the parameter spaces of three IDE models. Then, we plot the cosmic evolutions of Hubble diagram $H(z)$, deceleration diagram $q(z)$ and statefinder hierarchy $\{S_3^{(1)}, S_4^{(1)}\}$, and check whether or not these dark energy (DE) diagnosis can distinguish the differences among the results of different LCF. At last, we perform high-redshift cosmic age test using three old high redshift objects (OHRO), and explore the fate of the Universe.

Results: For all the IDE models, the impacts of different LCF on parameter estimation are as follows: (1) after considering the redshift-dependence of color-luminosity parameter β , the “SALT2” sample gives a smaller increasing rate of $\beta(z)$, while the SiFTO sample yields a larger increasing rate of $\beta(z)$; (2) the “Combined” sample gives a larger DE equation of state (EoS) w , while the “SiFTO” sample yields a smaller w ; (3) the effects of different LCF on other parameters are negligible. Moreover, we find that the impacts of different LCF are rather small and can not be distinguished by using the $H(z)$ diagram, the $q(z)$ diagram, and the age data of OHRO; in contrast, the statefinder hierarchy $\{S_3^{(1)}, S_4^{(1)}\}$ is a powerful tool that has the ability to distinguish the effects of different LCF. In addition, we infer, from the current observational data, how far we are from a cosmic doomsday in the worst case, and find that the “Combined” sample always gives a larger 2σ lower limit of the time interval between a “big rip” and today. Our method can be used to distinguish the differences among various cosmological observations.

Key words: cosmology: type Ia supernova, dark energy diagnosis, cosmic age test, fate of the Universe

1 INTRODUCTION

Type Ia supernovae (SNe Ia) are one of the most powerful probes to illuminate the mystery of cosmic acceleration (Riess et al. 1998; Perlmutter et al. 1999), which may be due to dark en-

ergy (DE), or modified gravity (MG). ¹ Along with the rapid progress of supernova (SN) cosmology, several high quality SN datasets were released in recent years, such as “SNLS” Astier et al. (2006), “Union” Kowalski et al. (2008), “Constitution” Hicken et al. (2009), “SDSS” Kessler et al. (2009), “Union2” Amanullah et al. (2010), “Union2.1” Suzuki et al. (2012), and “Pan-STARRS1”

* asiahu@itp.ac.cn

† mli@itp.ac.cn

‡ linan@itp.ac.cn

§ swang0229@mail.neu.edu.cn (Corresponding author)

¹ For recent reviews, see Frieman, Turner, & Huterer (2008); Caldwell & Kamionkowski (2009); Uzan (2010); Wang (2010); Li, Li, Wang, & Wang (2011); Weinberg et al. (2013).

Scolnic et al. (2014). In 2010, the Supernova Legacy Survey (SNLS) group released their three years data (Guy 2010). Soon after, combining these SN samples with various low- z to mid- z samples and making use of three different light-curve fitters (LCF), Conley et al. (2011) presented three SNLS3 data sets: “SALT2”, which consists of 473 SNe Ia; “SiFTO”, which consists of 468 SNe Ia; and “combined”, which consists of 472 SNe Ia. It should be mentioned that, the SNLS group treated two important quantities, stretch-luminosity parameter α and color-luminosity parameter β of SNe Ia, as free model parameters. In addition, the intrinsic scatter σ_{int} are fixed to ensure that $\chi^2/dof = 1$.

A critical challenge is the control of the systematic uncertainties of SNe Ia. One of the most important factors is the potential SN evolution. Previous studies on the SNLS3 (Wang & Wang 2013a), the Union2.1 (Mohlabeng & Ralston 2013), and the Pan-STARRS1 data sets (Scolnic et al. 2014) all indicated that α is still consistent with a constant, but β evolves along with redshift z at very high confidence level (CL); this conclusion has significant effects on parameter estimation of various cosmological models (Wang, Li & Zhang 2014; Wang, et al. 2014; Wang, Wang & Zhang 2014; Wang, et al. 2015). Besides, it was found that the intrinsic scatter σ_{int} also has the hint of redshift-dependence (Marriner et al. 2011) that will significantly affect the results of cosmology-fits. Another important factor is the models of LCF that are used to obtain SN sample. As mentioned above, based on three different LCF models, the SNLS3 group released three SN data sets: “SALT2”, “SiFTO” and “combined”. So far, only the “Combined” sample is studied extensively, both the “SALT2” and the “SiFTO” data sets are seldom taken into account in the literature. Although these three SNLS3 data sets had been used at the same time to study the Λ -cold-dark-matter (Λ CDM) model (Wang & Wang 2013a) and the holographic dark energy (HDE) model (Wang, et al. 2015), only the simplest discussions about the results of different LCF were given in these papers. Moreover, the effects of different LCF have not been studied in detail in the past. So the main aim of the present work is presenting a comprehensive and systematic investigation on the impacts of different SNLS3 LCF.

Here we adopt the w -cold-dark-matter (w CDM) model, which has a constant DE equation of state (EoS) w , in the background. In principle, there might exist a direct nongravitational interaction between DE and cold dark matter (CDM); such a dark sector interaction can provide an intriguing mechanism to solve the “coincidence problem” (Guo, Ohta, & Tsujikawa 2007; Li et al. 2009; He et al. 2010). In addition, as argued in Clarkson, Cortes, & Bassett (2007), owing to the degeneracy between the EoS of DE and the spatial curvature of the Universe, it is very important to include Ω_{k0} , which is the present fractional densities of spatial curvature, as a free parameter. Therefore, both the dark sector interaction and the spatial curvature are considered in the present work. Furthermore, to ensure that our study is insensitive to a specific form of interaction between dark sectors, three kinds of interaction terms are taken into account.

According to the previous studies on the potential SN evolution, we adopt a constant α and a linear $\beta(z) = \beta_0 + \beta_1 z$ in this work. Making use of the three SNLS3 data sets, as well as the latest Planck distance prior data (Wang & Wang 2013b), the galaxy clustering (GC) data extracted from Sloan Digital Sky Survey (SDSS) data release 7 (DR7) (Chuang & Wang 2012) and baryon oscillation spectroscopic survey (BOSS) (Chuang et al. 2013), and the direct measurement of Hubble constant H_0 from the Hubble Space Telescope (HST) observations (Riess et al. 2011), we constrain the parameter spaces of the three IDE models. Moreover, based on the

fitting results, we study the possibility of distinguishing the impacts of different LCF by using various DE diagnosis tools and cosmic age data.

We present our method in Section 2, our results in Section 3, and summarize and conclude in Section 4.

2 METHODOLOGY

In this section, firstly we review the theoretical framework of the interacting dark energy (IDE) models, then we briefly describe the observational data used in the present work, and finally we introduce the background knowledge about DE diagnosis and cosmic age.

2.1 Theoretical Models

In a non-flat Universe, the Friedmann equation is

$$3M_{pl}^2 H^2 = \rho_c + \rho_{de} + \rho_r + \rho_b + \rho_k, \quad (1)$$

where $H \equiv \dot{a}/a$ is the Hubble parameter, $a = (1+z)^{-1}$ is the scale factor of the Universe (we take today’s scale factor $a_0 = 1$), the dot denotes the derivative with respect to cosmic time t , $M_p^2 = (8\pi G)^{-1}$ is the reduced Planck mass, G is Newtonian gravitational constant, ρ_c , ρ_{de} , ρ_r , ρ_b and ρ_k are the energy densities of CDM, DE, radiation, baryon and spatial curvature, respectively. The reduced Hubble parameter $E(z) \equiv H(z)/H_0$ satisfies

$$E^2 = \Omega_{c0} \frac{\rho_c}{\rho_{c0}} + \Omega_{de0} \frac{\rho_{de}}{\rho_{de0}} + \Omega_{r0} \frac{\rho_r}{\rho_{r0}} + \Omega_{b0} \frac{\rho_b}{\rho_{b0}} + \Omega_{k0} \frac{\rho_k}{\rho_{k0}}, \quad (2)$$

where Ω_{c0} , Ω_{de0} , Ω_{r0} , Ω_{b0} and Ω_{k0} are the present fractional densities of CDM, DE, radiation, baryon and spatial curvature, respectively. Since $\Omega_{de0} = 1 - \Omega_{c0} - \Omega_{b0} - \Omega_{r0} - \Omega_{k0}$, Ω_{de0} is not an independent parameter. In addition, $\rho_r = \rho_{r0}(1+z)^4$, $\rho_b = \rho_{b0}(1+z)^3$, $\rho_k = \rho_{k0}(1+z)^2$, $\Omega_{r0} = \Omega_{m0}/(1+z_{eq})^4$, where $\Omega_{m0} = \Omega_{c0} + \Omega_{b0}$ and $z_{eq} = 2.5 \times 10^4 \Omega_{m0} h^2 (T_{cmb}/2.7 \text{ K})^{-4}$ (here we take $T_{cmb} = 2.7255 \text{ K}$).

In an IDE scenario, the energy conservation equations of CDM and DE satisfy

$$\dot{\rho}_c + 3H\rho_c = Q, \quad (3)$$

$$\dot{\rho}_{de} + 3H(\rho_{de} + p_{de}) = -Q, \quad (4)$$

where $p_{de} = w\rho_{de}$ is the pressure of DE, Q is the interaction term, which describes the energy transfer rate between CDM and DE. So far, the microscopic origin of interaction between dark sectors is still a puzzle. To study the issue of interaction, one needs to write down the possible forms of Q by hand. In this work we consider the following three cases:

$$Q_1 = 3\gamma H\rho_c, \quad (5)$$

$$Q_2 = 3\gamma H\rho_{de}, \quad (6)$$

$$Q_3 = 3\gamma H \frac{\rho_c \rho_{de}}{\rho_c + \rho_{de}}, \quad (7)$$

where γ is a dimensionless parameter describing the strength of interaction, $\gamma > 0$ means that energy transfers from DE to CDM, while $\gamma < 0$ implies that energy transfers from CDM to DE. Notice that the models with Q_1 and Q_2 have been widely studied in the literature (see, e.g., Guo, Ohta, & Tsujikawa 2007; Li et al. 2009; He et al. 2010); and the model with Q_3 , which can solve the early-time superhorizon instability and future unphysical CDM density problems at the same time, is proposed in Li & Zhang (2014),

For simplicity, hereafter we call them $Iw\text{CDM1}$ model, $Iw\text{CDM2}$ model, and $Iw\text{CDM3}$ model, respectively.

For the $Iw\text{CDM1}$ model, the solutions of Eqs. (3) and (4) are

$$\rho_c = \rho_{c0}(1+z)^{3(1-\gamma)}, \quad (8)$$

$$\rho_{de} = \frac{\gamma\rho_{c0}}{w+\gamma} \left((1+z)^{3(1+w)} - (1+z)^{3(1-\gamma)} \right) + \rho_{de0}(1+z)^{3(1+w)}. \quad (9)$$

Then we have

$$E(z) = \left(\Omega_{r0}(1+z)^4 + \Omega_{b0}(1+z)^3 + \Omega_{k0}(1+z)^2 + \Omega_{de0}(1+z)^{3(1+w)} + \Omega_{c0} \left(\frac{\gamma}{w+\gamma} (1+z)^{3(1+w)} + \frac{w}{w+\gamma} (1+z)^{3(1-\gamma)} \right) \right)^{1/2}. \quad (10)$$

For the $Iw\text{CDM2}$ model, the solutions of Eqs. (3) and (4) are

$$\rho_{de} = \rho_{de0}(1+z)^{3(1+w+\gamma)}, \quad (11)$$

$$\rho_c = \rho_{c0}(1+z)^3 + \frac{\gamma\rho_{de0}}{w+\gamma}(1+z)^3 - \frac{\gamma\rho_{de0}}{w+\gamma}(1+z)^{3(1+w+\gamma)}. \quad (12)$$

Then we get

$$E(z) = \left(\Omega_{r0}(1+z)^4 + (\Omega_{c0} + \Omega_{b0})(1+z)^3 + \Omega_{k0}(1+z)^2 + \Omega_{de0} \left(\frac{\gamma}{w+\gamma}(1+z)^3 + \frac{w}{w+\gamma}(1+z)^{3(1+w+\gamma)} \right) \right)^{1/2}. \quad (13)$$

For the $Iw\text{CDM3}$ model, Eqs. (3) and (4) still have analytical solutions

$$\rho_c = \rho_{c0}(1+z)^3 \left(\frac{\rho_{c0}}{\rho_{c0} + \rho_{de0}} + \frac{\rho_{de0}}{\rho_{c0} + \rho_{de0}}(1+z)^{3(w+\gamma)} \right)^{-\frac{\gamma}{w+\gamma}}, \quad (14)$$

$$\rho_{de} = \rho_{de0}(1+z)^{3(1+w+\gamma)} \left(\frac{\rho_{c0}}{\rho_{c0} + \rho_{de0}} + \frac{\rho_{de0}}{\rho_{c0} + \rho_{de0}}(1+z)^{3(w+\gamma)} \right)^{-\frac{\gamma}{w+\gamma}}. \quad (15)$$

Then we obtain

$$E(z) = \left(\Omega_{r0}(1+z)^4 + \Omega_{b0}(1+z)^3 + \Omega_{k0}(1+z)^2 + \Omega_{c0}C(z)(1+z)^3 + \Omega_{de0}C(z)(1+z)^{3(1+w+\gamma)} \right)^{1/2}. \quad (16)$$

where

$$C(z) = \left(\frac{\Omega_{c0}}{\Omega_{c0} + \Omega_{de0}} + \frac{\Omega_{de0}}{\Omega_{c0} + \Omega_{de0}}(1+z)^{3(w+\gamma)} \right)^{-\frac{\gamma}{w+\gamma}}. \quad (17)$$

For each model, the expression of $E(z)$ will be used to calculate the observational quantities appearing in the next subsection.

2.2 Observational Data

In the present work, we use the three SNLS3 data sets (i.e. “combined”, “SALT2”, and “SiFTO”). In the following, we briefly introduce how to include these three data sets into the χ^2 analysis.

For a set of N SNe with correlated errors, the χ^2 function is given by

$$\chi_{SN}^2 = \Delta \mathbf{m}^T \cdot \mathbf{C}^{-1} \cdot \Delta \mathbf{m}, \quad (18)$$

where \mathbf{C} is a $N \times N$ covariance matrix (For the details of constructing the corresponding covariance matrix, see Conley et al. (2011)), and $\Delta \mathbf{m} \equiv m_B - m_{\text{mod}}$ is a vector with N components. Here m_B is the rest-frame peak B-band magnitude of the SN. Adopting a constant α and a linear $\beta(z) = \beta_0 + \beta_1 z$, the predicted magnitude of an SN becomes

$$m_{\text{mod}} = 5 \log_{10} \mathcal{D}_L(z) - \alpha(s-1) + \beta(z)\mathcal{C} + \mathcal{M}. \quad (19)$$

The luminosity distance $\mathcal{D}_L(z)$ is defined as

$$\mathcal{D}_L(z) \equiv H_0(1+z_{\text{hel}})r(z), \quad (20)$$

where z and z_{hel} are the CMB restframe and heliocentric redshifts of SN, $r(z) = H_0^{-1} |\Omega_{k0}|^{-1/2} \text{sinn}(|\Omega_{k0}|^{1/2} \Gamma(z))$, $\Gamma(z) = \int_0^z \frac{dz'}{E(z')}$, and $\text{sinn}(x) = \sin(x)$, x , $\sinh(x)$ for $\Omega_{k0} < 0$, $\Omega_{k0} = 0$, and $\Omega_{k0} > 0$ respectively. Here s and \mathcal{C} are stretch measure and color measure for the SN light curve, \mathcal{M} is a parameter representing some combination of SN absolute magnitude M and Hubble constant H_0 .

It must be emphasized that, in order to include host-galaxy information in the cosmological fits, Conley et al. (2011) split the SNLS3 sample based on host-galaxy stellar mass at $10^{10} M_\odot$, and made \mathcal{M} to be different for the two samples. So there are two values of \mathcal{M} (i.e. \mathcal{M}_1 and \mathcal{M}_2) for the SNLS3 data. Moreover, Conley et al. removed \mathcal{M}_1 and \mathcal{M}_2 from cosmology-fits by analytically marginalizing over them (for more details, see the appendix C of Conley et al. (2011)). In the present work, we just follow the recipe of Conley et al. (2011), and do not treat \mathcal{M} as model parameter.

To improve the cosmological constraints, we also use some other cosmological observations, including the Planck distance prior data Wang & Wang (2013b), the GC data extracted from SDSS DR7 Chuang & Wang (2012) and BOSS Chuang et al. (2013), as well as the direct measurement of Hubble constant $H_0 = 73.8 \pm 2.4 \text{ km/s/Mpc}$ from the HST observations Riess et al. (2011). For the details of including these observational data into the χ^2 analysis, see Wang, Li & Zhang (2014); Wang, et al. (2014). It should be mentioned that, in this paper we just use the purely geometric measurements, and do not consider the cosmological perturbations in the IDE models. As analyzed in Li, Zhang, & Zhang (2014), adopting a new framework for calculating the perturbations, the cosmological perturbations will always be stable in all IDE models. Therefore, the use of the Planck distance prior is sufficient for our purpose. Now the total χ^2 function is

$$\chi^2 = \chi_{SN}^2 + \chi_{CMB}^2 + \chi_{GC}^2 + \chi_{H_0}^2. \quad (21)$$

Finally, we perform an MCMC likelihood analysis using the “CosmoMC” package Lewis & Bridle (2002).

2.3 Dark Energy Diagnosis and Cosmic Age

This subsection consists of two parts. Firstly, we introduce the tools of DE diagnosis, including the Hubble parameter $H(z)$, the deceleration parameter $q(z)$, and the statefinder hierarchy $\{S_3^{(1)}, S_4^{(1)}\}$ Arabsalmani & Sahni (2009). Then, we discuss the issues about cosmic age, including the high-redshift cosmic age test and the fate of the Universe.

Let us introduce the DE diagnosis tools first. The scale factor of the Universe a can be Taylor expanded around today’s cosmic age t_0 as follows:

$$a(t) = 1 + \sum_{n=1}^{\infty} \frac{A_n}{n!} [H_0(t-t_0)]^n, \quad (22)$$

where

$$A_n = \frac{a(t)^{(n)}}{a(t)H^n}, \quad n \in N, \quad (23)$$

with $a(t)^{(n)} = d^n a(t)/dt^n$. The Hubble parameter $H(z)$ contain

the information of the first derivative of $a(t)$. Based on the Baryon Acoustic Oscillations (BAO) measurements from the SDSS data release 9 and data release 11, Samushia et al. (2013) gave $H_{0.57} \equiv H(z = 0.57) = 92.4 \pm 4.5 \text{ km/s/Mpc}$, while Delubac et al. (2014) obtained $H_{2.34} \equiv H(z = 2.34) = 222 \pm 7 \text{ km/s/Mpc}$. These two $H(z)$ data points will be used to compare the theoretical predictions of IDE models. In addition, the deceleration parameter q is given by

$$q = -A_2 = -\frac{\ddot{a}}{aH^2}, \quad (24)$$

which contains the information of the second derivatives of $a(t)$. For the Λ CDM model, $A_2|_{\Lambda\text{CDM}} = 1 - \frac{3}{2}\Omega_m$, $A_3|_{\Lambda\text{CDM}} = 1$, $A_4|_{\Lambda\text{CDM}} = 1 - \frac{3^2}{2}\Omega_m$, where $\Omega_m = \Omega_c + \Omega_b$ is the fractional density of matter. The statefinder hierarchy, S_n , is defined as Arabalmani & Sahni (2009):

$$S_2 = A_2 + \frac{3}{2}\Omega_m, \quad (25)$$

$$S_3 = A_3, \quad (26)$$

$$S_4 = A_4 + \frac{3^2}{2}\Omega_m, \quad (27)$$

The reason for this redefinition is to peg the statefinder at unity for Λ CDM during the cosmic expansion,

$$S_n|_{\Lambda\text{CDM}} = 1. \quad (28)$$

This equation defines a series of null diagnostics for Λ CDM when $n \geq 3$. By using this diagnostic, we can easily distinguish the Λ CDM model from other DE models. Because of $\Omega_m|_{\Lambda\text{CDM}} = \frac{2}{3}(1+q)$, when $n \geq 3$, statefinder hierarchy can be rewritten as:

$$S_3^{(1)} = A_3, \quad (29)$$

$$S_4^{(1)} = A_4 + 3(1+q), \quad (30)$$

where the superscript (1) is to discriminate between $S_n^{(1)}$ and S_n . In this paper, we use the statefinder hierarchy $\{S_3^{(1)}, S_4^{(1)}\}$ to diagnose the IDE models.

Now, let us turn to the issues about cosmic age. The age of the Universe at redshift z is given by

$$t(z) = \int_z^\infty \frac{d\tilde{z}}{(1+\tilde{z})H(\tilde{z})}. \quad (31)$$

In history, the cosmic age problem played an important role in the cosmology Alcaniz & Lima (1999); Lan et al. (2010); Liu & Zhang (2014)). Obviously, the Universe cannot be younger than its constituents. In other words, the age of the universe at any high redshift z cannot be younger than its constituents at the same redshift. There are some old high redshift objects (OHRO) considered extensively in the literature. For instance, the 3.5 Gyr old galaxy LBDS 53W091 at redshift $z = 1.55$ Dunlop et al. (1996), the 4.0 Gyr old galaxy LBDS 53W069 at redshift $z = 1.43$ Dunlop (1999), and the old quasar APM 08279+5255, whose age is estimated to be 2.0 C 3.0 Gyr, at redshift $z = 3.91$ Hasinger, Schartel, & Komossa (2002). In the literature, the age data of these three OHRO (i.e. $t_{1.43} \equiv t(z = 1.43) = 4.0 \text{ Gyr}$, $t_{1.55} \equiv t(z = 1.55) = 3.5 \text{ Gyr}$ and $t_{3.91} \equiv t(z = 3.91) = 2.0 \text{ Gyr}$) have been extensively used to test various cosmological models (see e.g. Alcaniz, Lima & Cunha (2003); Wei & Zhang (2007); Wang & Zhang (2008); Wang, Li & Li (2010); Yan, Liu & Wei (2014)). In the present work, we will use these three age data to test the IDE models.

Another interesting topic is the fate of the Universe. The future of the Universe depends on the property of DE. If the Universe is dominated by a quintessence Caldwell, Dave & Steinhardt

(1998); Zlatev, Wang & Steinhardt (1999) or a cosmological constant (for this case, ρ_{de} will decrease with time t or remain a constant), the expansion of the Universe will continue forever, and all the structures that are currently gravitationally bound will remain unaffected forever. If the Universe is dominated by a phantom Caldwell (2002); Caldwell, Kamionkowski & Weinberg (2003) (for this case, ρ_{de} will always increase with time t), eventually the repulsive gravity of DE will become large enough to tear apart all the structures, and the Universe will finally encounter a doomsday, i.e. the so-called “big rip” (BR). Setting $x = -\ln(1+z)$, we can get the time interval between a BR and today

$$t_{BR} - t_0 = \int_0^\infty \frac{dx}{H(x)}, \quad (32)$$

where t_{BR} denotes the time of BR. It is obvious that, for a Universe dominated by a quintessence or a cosmological constant, this integration is infinity; and for a Universe dominated by a phantom, this integration is convergence. We would like to infer, from the current observational data, how far we are from a cosmic doomsday in the worst case. So in this work we calculate the 2σ lower limits of $t_{BR} - t_0$ for all the IDE models.

3 RESULT

In this section, firstly we present the fitting results of the three IDE models, then we show the cosmic evolutions of Hubble parameter $H(z)$, deceleration parameter $q(z)$, and statefinder hierarchy $\{S_3^{(1)}, S_4^{(1)}\}$ according to the fitting results, and finally we perform the high-redshift cosmic age test and discuss the possible fate of the Universe.

3.1 Cosmology Fits

In table 1, we give the fitting results of the three IDE models, where both the best-fit values and the 1σ errors of various parameters are listed. From this table we see that, for all the IDE models, β significantly deviates from a constant, consistent with the results of Wang, et al. (2014); in addition, the current cosmological observations favor a positive Ω_{k0} (corresponding to an open Universe) and a negative γ (denoting energy transfers from CDM to DE) at 1σ CL. Although the best-fit results of w given by the three LCF are always less than -1 , $w = -1$ is still consistent with the current cosmological observations at 1σ CL. Moreover, we check the impacts of different SNLS3 LCF on parameter estimation and find that for all the IDE models: (1) The “SALT2” sample gives a larger α and a smaller β_1 ; in contrast, the “SiFTO” sample yields a smaller α and a larger β_1 . (2) The “Combined” sample gives a larger w and a larger Ω_{k0} , while the “SiFTO” sample yields a smaller w . (3) The effects of different LCF on other parameters are negligible.

Let us discuss the fitting results with more details. In Fig. 1, we plot the 1σ confidence regions of $\beta(z)$ at redshift region $[0, 1]$ for the three IDE models. We find that, for all the IDE models, the trends of $\beta(z)$ given by different LCF are essentially the same. Furthermore, the SALT2 sample gives a smaller increasing rate of $\beta(z)$, while the SiFTO sample yields a larger increasing rate of $\beta(z)$. These results are consistent with the results of the Λ CDM model Wang & Wang (2013a) and the HDE model Wang, et al. (2015), implying that the effects of different LCF are insensitive to the DE models considered in the background.

In Fig. 2, we plot the probability contours at the 1σ and 2σ CL in the γ - w plane, for the three IDE models. The best-fit values

Table 1. Fitting results for the three IDE models, where both the best-fit values and the 1σ errors of various parameters are listed. “Combined”, “SALT2” and “SiFTO” represent the SN(Combined)+CMB+GC+ H_0 , the SN(SALT2)+CMB+GC+ H_0 and the SN(SiFTO)+CMB+GC+ H_0 data, respectively.

Parameter	IwCDM1			IwCDM2			IwCDM3		
	Combined	SALT2	SiFTO	Combined	SALT2	SiFTO	Combined	SALT2	SiFTO
α	$1.412^{+0.069}_{-0.055}$	$1.605^{+0.097}_{-0.143}$	$1.339^{+0.067}_{-0.022}$	$1.435^{+0.044}_{-0.090}$	$1.537^{+0.142}_{-0.069}$	$1.352^{+0.050}_{-0.029}$	$1.417^{+0.058}_{-0.060}$	$1.585^{+0.121}_{-0.136}$	$1.384^{+0.023}_{-0.070}$
β_0	$1.512^{+0.148}_{-0.305}$	$2.083^{+0.092}_{-0.255}$	$1.453^{+0.207}_{-0.226}$	$1.469^{+0.221}_{-0.249}$	$2.058^{+0.127}_{-0.206}$	$1.491^{+0.227}_{-0.273}$	$1.398^{+0.251}_{-0.174}$	$2.014^{+0.222}_{-0.203}$	$1.564^{+0.163}_{-0.343}$
β_1	$4.926^{+0.768}_{-0.438}$	$3.587^{+0.753}_{-0.294}$	$5.246^{+0.644}_{-0.525}$	$4.949^{+0.712}_{-0.568}$	$3.686^{+0.630}_{-0.391}$	$5.180^{+0.749}_{-0.573}$	$5.149^{+0.725}_{-0.789}$	$3.824^{+0.604}_{-0.606}$	$5.329^{+0.727}_{-0.739}$
Ω_{c0}	$0.245^{+0.009}_{-0.010}$	$0.242^{+0.010}_{-0.009}$	$0.242^{+0.010}_{-0.011}$	$0.243^{+0.009}_{-0.011}$	$0.240^{+0.010}_{-0.009}$	$0.238^{+0.011}_{-0.008}$	$0.241^{+0.011}_{-0.008}$	$0.238^{+0.010}_{-0.010}$	$0.239^{+0.012}_{-0.009}$
Ω_{b0}	$0.041^{+0.002}_{-0.002}$	$0.041^{+0.002}_{-0.002}$	$0.040^{+0.002}_{-0.001}$	$0.042^{+0.001}_{-0.002}$	$0.042^{+0.001}_{-0.002}$	$0.042^{+0.002}_{-0.002}$	$0.042^{+0.002}_{-0.002}$	$0.042^{+0.001}_{-0.002}$	$0.041^{+0.002}_{-0.002}$
Ω_{k0}	$0.0092^{+0.0035}_{-0.0042}$	$0.0067^{+0.0047}_{-0.0030}$	$0.0073^{+0.0041}_{-0.0041}$	$0.0173^{+0.0151}_{-0.0112}$	$0.0165^{+0.0126}_{-0.0090}$	$0.0159^{+0.0150}_{-0.0091}$	$0.0199^{+0.0111}_{-0.0109}$	$0.0138^{+0.0161}_{-0.0073}$	$0.0170^{+0.0136}_{-0.0103}$
γ	$-0.0050^{+0.0025}_{-0.0019}$	$-0.0044^{+0.0021}_{-0.0021}$	$-0.0050^{+0.0033}_{-0.0014}$	$-0.0288^{+0.0203}_{-0.0330}$	$-0.0290^{+0.0195}_{-0.0247}$	$-0.0288^{+0.0183}_{-0.0309}$	$-0.0684^{+0.0409}_{-0.0561}$	$-0.0483^{+0.0304}_{-0.0701}$	$-0.0647^{+0.0420}_{-0.0664}$
w	$-1.002^{+0.042}_{-0.060}$	$-1.033^{+0.044}_{-0.050}$	$-1.044^{+0.063}_{-0.046}$	$-1.044^{+0.038}_{-0.056}$	$-1.069^{+0.057}_{-0.043}$	$-1.075^{+0.054}_{-0.041}$	$-1.035^{+0.037}_{-0.058}$	$-1.056^{+0.055}_{-0.056}$	$-1.066^{+0.058}_{-0.053}$
h	$0.738^{+0.015}_{-0.014}$	$0.735^{+0.014}_{-0.013}$	$0.742^{+0.010}_{-0.022}$	$0.726^{+0.018}_{-0.010}$	$0.730^{+0.015}_{-0.013}$	$0.732^{+0.015}_{-0.015}$	$0.733^{+0.012}_{-0.013}$	$0.727^{+0.022}_{-0.009}$	$0.733^{+0.015}_{-0.014}$

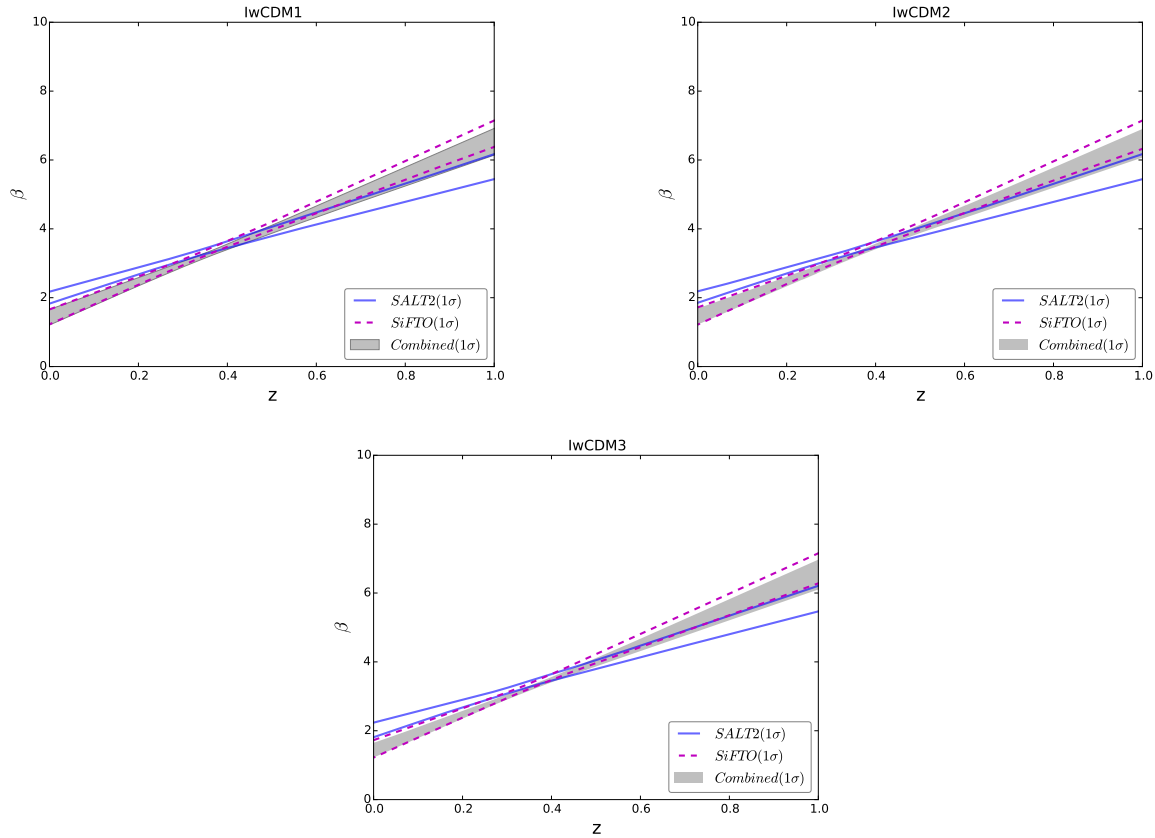


Figure 1. (color online). The 1σ confidence regions of $\beta(z)$ for the IwCDM1 (upper left panel), the IwCDM2 (upper right panel) and the IwCDM3 (lower panel) model. “Combined” (gray filled regions), “SALT2” (blue solid lines), and “SiFTO” (purple dashed lines) denote the results given by the SN(Combined)+CMB+GC+ H_0 , the SN(SALT2)+CMB+GC+ H_0 , and the SN(SiFTO)+CMB+GC+ H_0 data, respectively.

of $\{\gamma, w\}$ of the “Combined”, the “SALT2” and the “SiFTO” data are marked as a black square, a red triangle and a green diamond, respectively. For comparison, the fixed point $\{\gamma, w\} = \{0, -1\}$ for the Λ CDM model is also marked as a blue round dot. A most obvious feature of this figure is that, for all the IDE models, the fixed point $\{0, -1\}$ of the Λ CDM model is outside the 1σ contours given by the three data sets, implying the importance of considering the interaction between dark sectors; besides, the Λ CDM model is still consistent with the observational data at 2σ CL. In addition, for the IwCDM2 model, the best-fit points given by the “SALT2” and the “SiFTO” data are very close. Moreover, according to the

evolution behaviors of ρ_{de} (see Eqs. 9, 11 and 15) at $z \rightarrow -1$, we divide these γ - w planes into two regions: the region above the dividing line denotes a quintessence dominated Universe (without big rip), and the region below the dividing line represents a phantom dominated Universe (with big rip). We can see that, although all the best-fit points given by the three data sets correspond to a phantom, both the phantom, the quintessence and the cosmological constant are consistent with the current cosmological observations at 2σ CL. This means that the current observational data are still too limited to indicate the nature of DE.

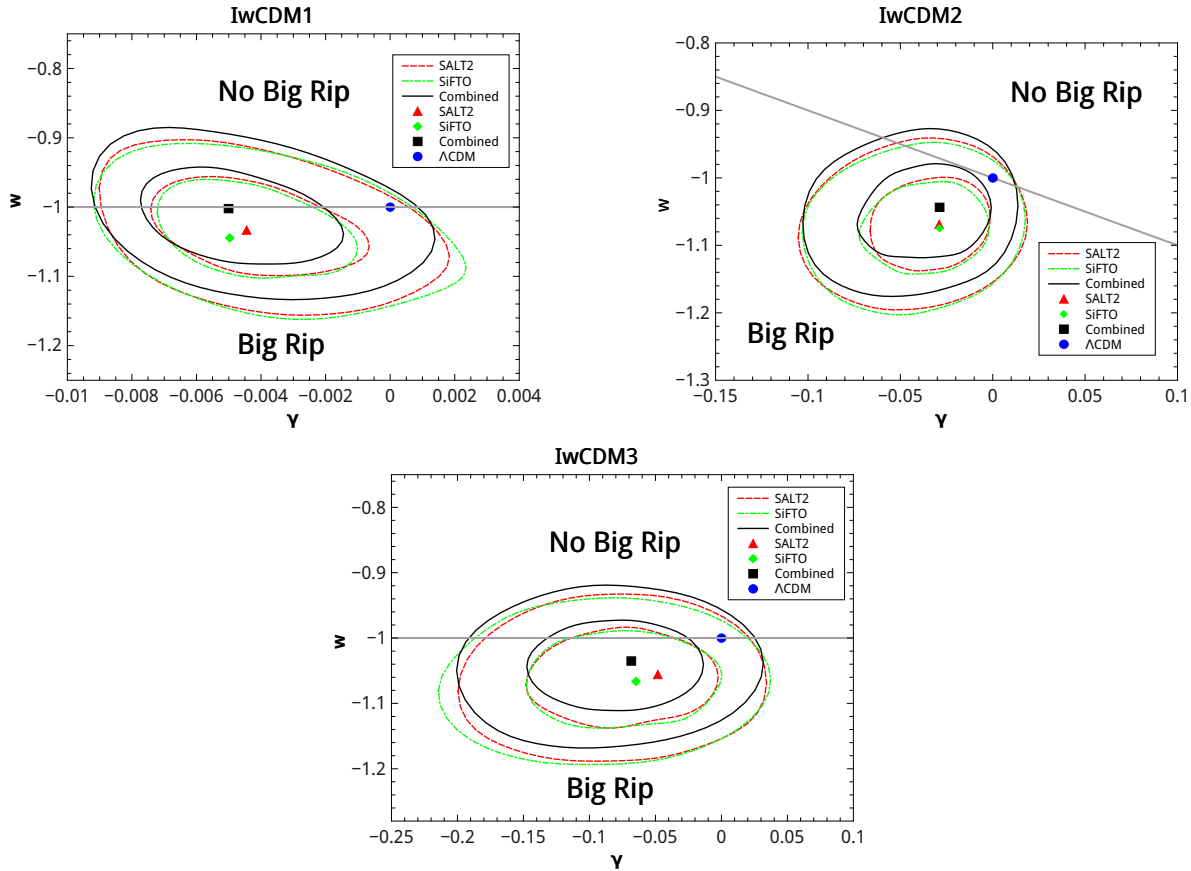


Figure 2. (color online). Probability contours at the 1σ and 2σ CL in the γ - w plane, for the $Iw\text{CDM1}$ (upper left panel), the $Iw\text{CDM2}$ (upper right panel) and the $Iw\text{CDM3}$ (lower panel) model. “Combined” (black solid lines), “SALT2” (red dashed lines), and “SiFTO” (green dash-dotted lines) denote the results given by the $\text{SN(Combined)+CMB+GC+}H_0$, the $\text{SN(SALT2)+CMB+GC+}H_0$, and the $\text{SN(SiFTO)+CMB+GC+}H_0$ data, respectively. Furthermore, the best-fit values of $\{\gamma, w\}$ of the “Combined”, the “SALT2” and the “SiFTO” data are marked as a black square, a red triangle and a green diamond, respectively. To make a comparison, the fixed point $\{\gamma, w\} = \{0, -1\}$ for the ΛCDM model is also marked as a blue round dot. The gray solid line divides the panel into two regions: the region above the dividing line denotes a quintessence dominated Universe (without big rip), and the region below the dividing line represents a phantom dominated Universe (with big rip).

3.2 Hubble Parameter, Deceleration Parameter and Statefinder Hierarchy

The 1σ confidence regions of Hubble parameter $H(z)$ at redshift region $[0, 4]$ for the three IDE models are plotted in Fig. 3, where the two $H(z)$ data points, $H_{0.57}$ and $H_{2.34}$, are also marked by diamonds with error bars for comparison. We find that the data point $H_{0.57}$ can be easily accommodated in the IDE models, but the data point $H_{2.34}$ significantly deviates from the 1σ regions of all the IDE models. In other words, the measurement of $H_{2.34}$ is in considerable tension with other cosmological observations and this result is consistent with the conclusion of Sahni, Shafieloo & Starobinsky (2014). In addition, the 1σ confidence regions of $H(z)$ given by different LCF are almost overlap; this means that using $H(z)$ diagram is almost impossible to distinguish the differences among different LCF.

In Fig. 4, we plot the 1σ confidence regions of deceleration parameter $q(z)$ at redshift region $[0, 4]$, for the three IDE models. Again, we see that the 1σ confidence regions of $q(z)$ given by different LCF are almost overlap. This implies that using $q(z)$ diagram also has great difficulty to distinguish the differences among different LCF.

Based on the best-fit results listed in table 1, in Fig. 5 we plot

the evolutionary trajectories of $\{S_3^{(1)}, S_4^{(1)}\}$ at redshift region $[0, 4]$ for all the IDE models. The current values of $\{S_3^{(1)}, S_4^{(1)}\}$ given by the “Combined”, the “SALT2” and the “SiFTO” data are marked as a black square, a red triangle and a green diamond, respectively. To make a comparison, the fixed point $\{S_3^{(1)}, S_4^{(1)}\} = \{1, 1\}$ for the ΛCDM model is also marked as a blue round dot. The difference between two models is measured by the distance between their fixed points of today. In addition, the arrows indicate the evolution directions of the models. The most feature of this figure is that, the evolution trajectories of $\{S_3^{(1)}, S_4^{(1)}\}$ given by different LCF are significantly different for all the IDE models; this means that statefinder hierarchy $\{S_3^{(1)}, S_4^{(1)}\}$ is a powerful tool that has the ability to distinguish the effects of different LCF. For the $Iw\text{CDM2}$ model, the evolutionary trajectories of $\{S_3^{(1)}, S_4^{(1)}\}$ given by the “SALT2” and the “SiFTO” data are very close, because the best-fit results given by the “SALT2” data are very close to that given by the “SiFTO” data (see Fig. 2); this unusual result does not affect the overall conclusion of the present work. In addition, for all the IDE models, the square given by the “combined” sample is more close to the round dot of the ΛCDM model, implying that the cosmological fitting results given by the combined sample are closer to the ΛCDM model.

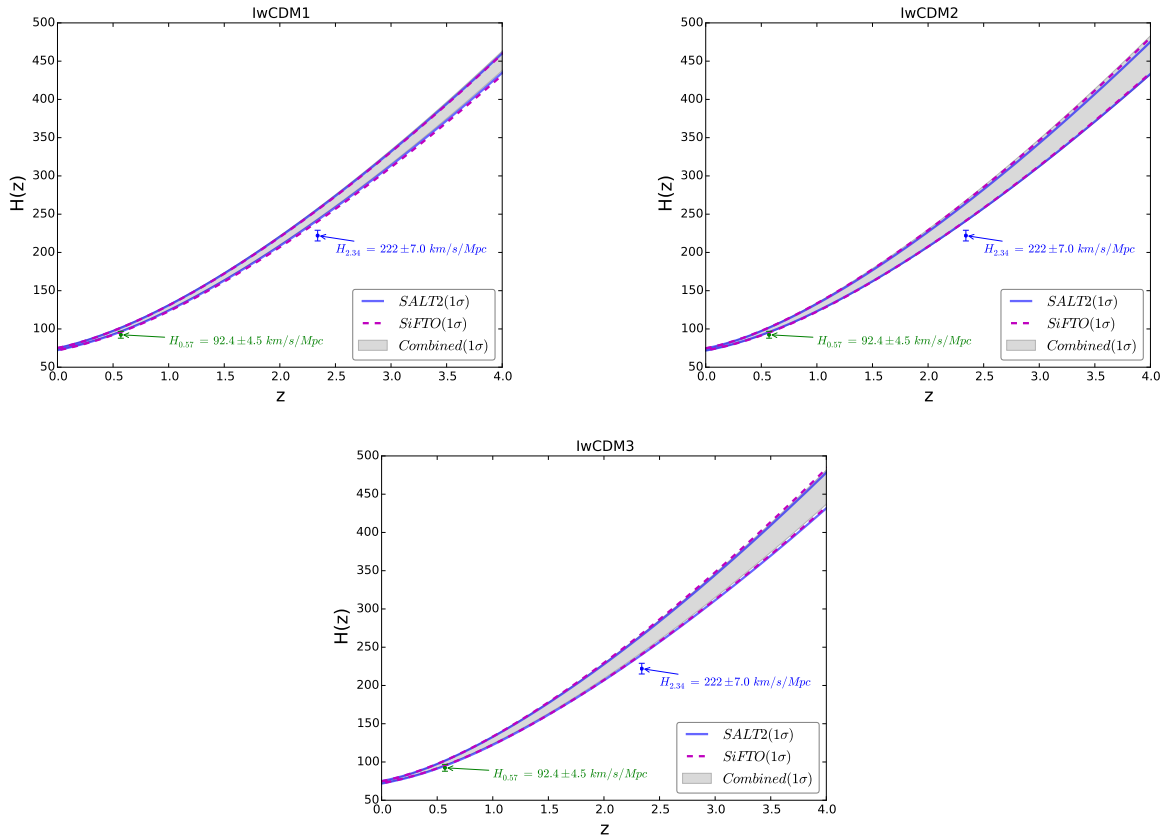


Figure 3. (color online). The 1σ confidence regions of Hubble parameter $H(z)$ at redshift region $[0, 4]$, for the $IwCDM1$ (upper left panel), the $IwCDM2$ (upper right panel) and the $IwCDM3$ (lower panel) model, where the data points of $H_{0.57}$ and $H_{2.34}$ are also marked by diamonds with error bars for comparison. “Combined” (gray filled regions), “SALT2” (blue solid lines), and “SiFTO” (purple dashed lines) denote the results given by the SN(Combined)+CMB+GC+ H_0 , the SN(SALT2)+CMB+GC+ H_0 , and the SN(SiFTO)+CMB+GC+ H_0 data, respectively.

3.3 High-Redshift Cosmic Age Test and Fate of The Universe

The 2σ confidence regions of cosmic age $t(z)$ at redshift region $[0, 4]$ for the three IDE models are plotted in Fig. 6, where the three $t(z)$ data points, $t_{1.43}$, $t_{1.55}$ and $t_{3.91}$, are also marked by Squares for comparison. We find that both $t_{1.43}$ and $t_{1.55}$ can be easily accommodated in the IDE models, but the position of $t_{3.91}$ is significantly higher than the 2σ upper bounds of the IDE models. In other words, the existence of the old quasar APM 08279+5255 can not be explained in the frame of IDE model. This result is consistent with the conclusions of pervious studies Alcaniz, Lima & Cunha (2003); Wei & Zhang (2007); Wang & Zhang (2008); Wang, Li & Li (2010); Yan, Liu & Wei (2014). In addition, the 2σ regions of $t(z)$ given by different LCF are almost overlap, showing that the impacts of different LCF can not be distinguished by using the age data of OHRO.

We want to infer how far we are from a cosmic doomsday in the worst case. So in Fig. 7, we plot the 2σ lower limits of the time interval $t - t_0$ between a future moment and today, for the three IDE models. Moreover, the 2σ lower limit values of $t_{BR} - t_0$ given by the three LCF are also marked on this figure. All the evolution curves of $t - t_0$ tend to the corresponding convergence values at $-\ln(1+z) \simeq 20$. The most important factor of determining $t_{BR} - t_0$ is the EoS w . In a phantom dominated Universe, a smaller w corresponds to a larger increasing rate of ρ_{de} ; this means that all the gravitationally bound structures will be torn apart in a

shorter time, and the Universe will encounter a cosmic doomsday in a shorter time, too. Among the three IDE models, the $IwCDM1$ model always gives a larger w (see table 1), and thus also gives a larger 2σ lower limit value of $t_{BR} - t_0$. Similarly, among the three SNLS3 LCF data, the “combined” sample always gives a larger w (see table 1), and thus also gives a larger value of $t_{BR} - t_0$.

4 SUMMARY AND DISCUSSION

As is well known, different LCF will yield different SN sample. In 2011, based on three different LCF, the SNLS3 group Conley et al. (2011) released three kinds of SN samples, i.e., “SALT2”, “SiFTO” and “combined”. So far, only the SNLS3 “Combined” sample is studied extensively, both the “SALT2” and the “SiFTO” data sets are seldom taken into account in the literature. Although these three SNLS3 data sets were used at the same time to study some DE models, the effects of different LCF have not been studied in detail in the past. So the main aim of the present work is presenting a comprehensive and systematic investigation on the impacts of different SNLS3 LCF.

We have used the three SNLS3 data sets, as well as the observational data from the CMB, the GC, and the direct measurement of Hubble constant H_0 , to constrain the parameter spaces of three IDE models. According to the results of cosmology-fits, we have plotted the cosmic evolutions of Hubble parameter $H(z)$, deceleration

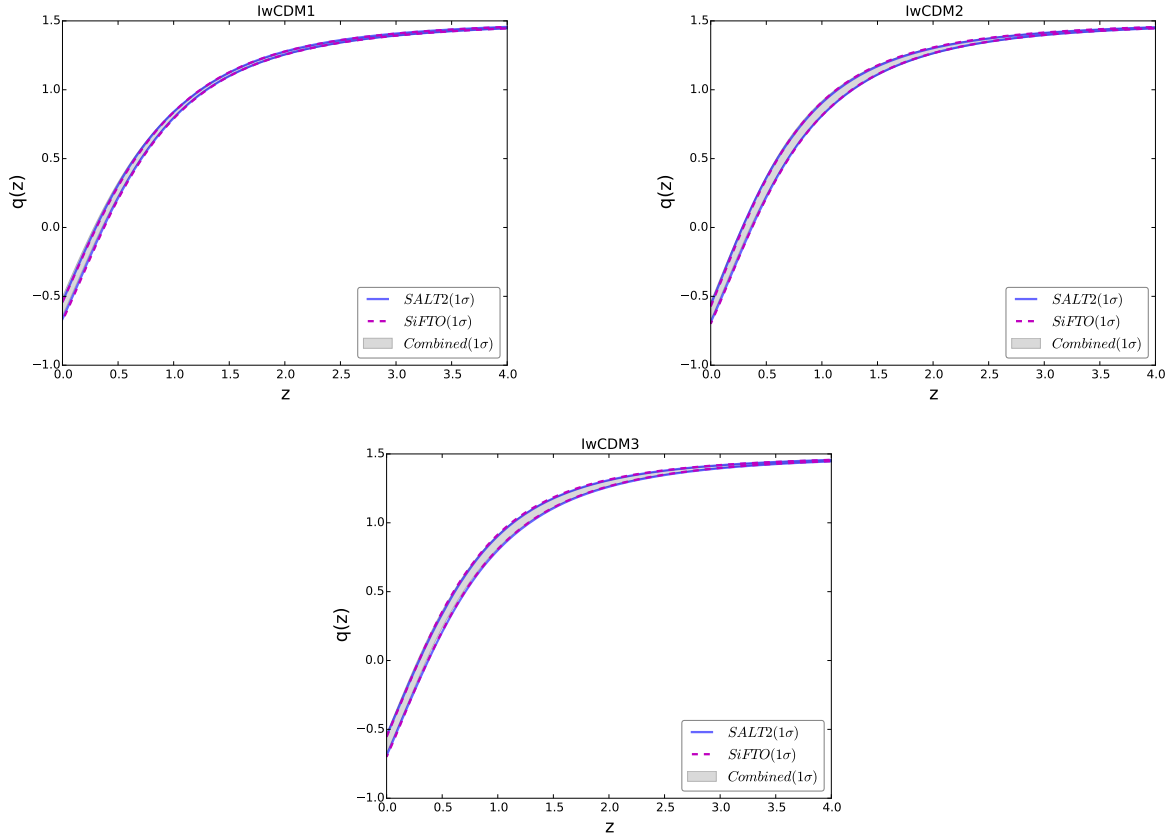


Figure 4. (color online). The 1σ confidence regions of deceleration parameter $q(z)$ at redshift region $[0, 4]$ for the $IwCDM1$ (upper left panel), the $IwCDM2$ (upper right panel) and the $IwCDM3$ (lower panel) model. “Combined” (gray filled regions), “SALT2” (blue solid lines), and “SiFTO” (purple dashed lines) denote the results given by the SN(Combined)+CMB+GC+ H_0 , the SN(SALT2)+CMB+GC+ H_0 , and the SN(SiFTO)+CMB+GC+ H_0 data, respectively.

parameter $q(z)$, and statefinder hierarchy $\{S_3^{(1)}, S_4^{(1)}\}$, and have checked whether or not these DE diagnoses can distinguish the differences among the results of different LCF. Furthermore, we have performed high-redshift cosmic age test using three OHRO, and have explored the fate of the Universe.

We find that for all the IDE models: (1) the “SALT2” sample gives a smaller increasing rate of $\beta(z)$, while the SiFTO sample yields a larger increasing rate of $\beta(z)$ (see Fig. 1); (2) the “Combined” sample gives a larger w , while the “SiFTO” sample yields a smaller w (see Fig. 2); (3) the effects of different LCF on other parameters are negligible (see table 1). Besides, we find that the Λ CDM model is inconsistent with the three SNLS3 samples at 1σ CL, but is still consistent with the observational data at 2σ CL.

Moreover, we find that the impacts of different LCF are rather small and can not be distinguished by using the $H(z)$ diagram (see Fig. 3), the $q(z)$ diagram (see Fig. 4), and the age data of OHRO (see Fig. 6); in contrast, statefinder hierarchy $\{S_3^{(1)}, S_4^{(1)}\}$ is a powerful tool that has the ability to distinguish the effects of different LCF (see Fig. 5). In addition, we infer how far we are from a cosmic doomsday in the worst case, and find that the “Combined” sample always gives a larger 2σ lower limit of $t_{BR} - t_0$ (see Fig. 7).

Since the conclusions listed above hold true for all the IDE models, we can conclude that the impacts of different LCF are insensitive to the specific forms of interaction between dark sectors. Moreover, our method can be used to distinguish the differences among various cosmological observations.

For simplicity, in the present work we only adopt a constant w ,

and do not consider the possible evolution of w . In the literature, the dynamical evolution of EoS are often explored by assuming a specific ansatz for $w(z)$ Chevallier & Polarski (2001); Linder (2003); Gerke, & Efstathiou (2002); Wetterich (2004); Jassal, Bagla, & Padmanabhan (2005), or by adopting a binned parametrization Huterer, & Starkman (2003); Huterer, & Cooray (2005); Huang et al. (2009); Wang, Li & Li (2011); Li et al. (2011); Gong, Gao, & Zhu (2013). To further study the impacts of various systematic uncertainties of SNe Ia on parameter estimation, we will extend our investigation to the case of a time-varying w in the future.

As seen in Figs. 3 and 6, two data points, $H_{2.34}$ and $t_{3.91}$, are in considerable tension with other cosmological observations. Although the data points $H_{2.34}$ and $t_{3.91}$ are obtained from two completely different approaches, both of them require a smaller increasing rate of Hubble parameter $H(z)$. If one can construct a theoretical model that reasonably gives a smaller $H(z)$ at high redshift range, these two anomalous data points can be accommodated at the same time.

In a recent paper Betoule et al. (2014), based on the improved SALT2 LCF, Betoule et al presented a latest SN data set (“joint light-curve analysis” (JLA) data set), which consists of 740 SNe Ia. Adopting a constant α and a constant β , Betoule et al. found $\Omega_{m0} = 0.295 \pm 0.034$ for a flat Λ CDM model; this result is different from the result of SNLS3 data, but is consistent with the results of Planck Ade et al. (2014). It would be interesting to apply our method to compare the differences between the SNLS3 and the JLA sample. These issues will be studied in future works.

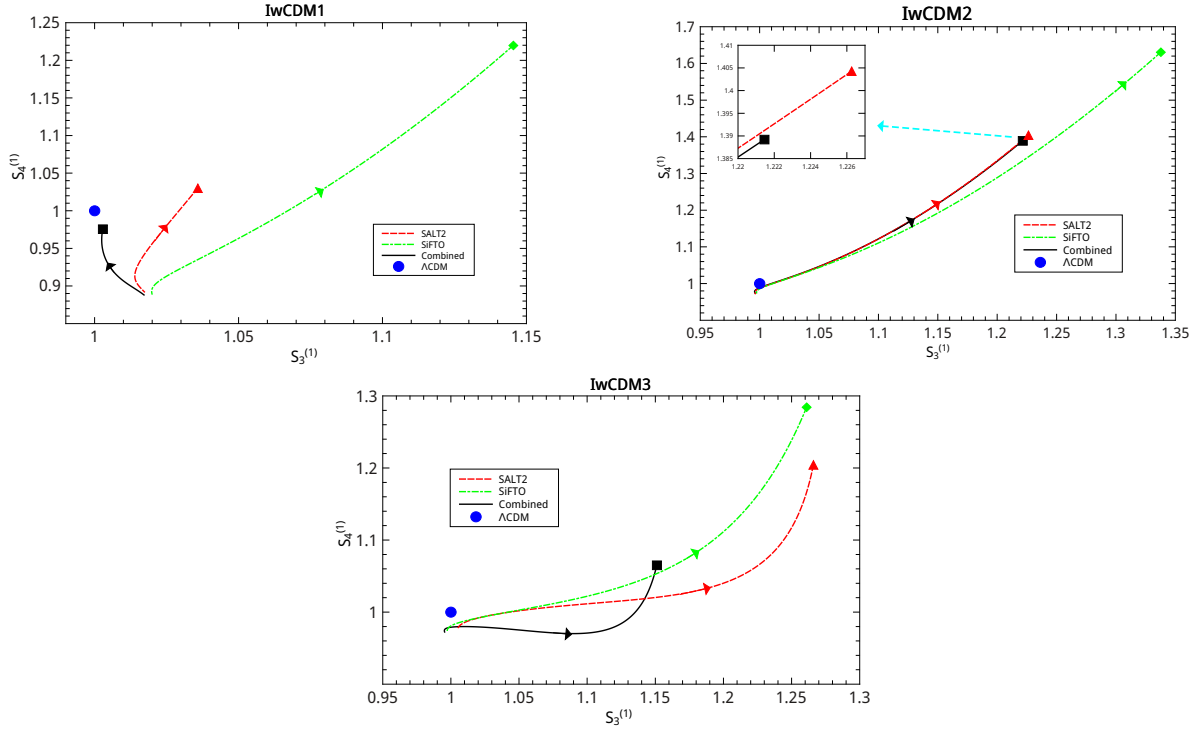


Figure 5. (color online). The evolutionary trajectories of $\{S_3^{(1)}, S_4^{(1)}\}$ at redshift region $[0, 4]$, for the $IwCDM1$ (upper left panel), the $IwCDM2$ (upper right panel) and the $IwCDM3$ (lower panel) model. “Combined” (black solid line), “SALT2” (red dashed lines), and “SiFTO” (green dash-dotted lines) denote the results given by the SN(Combined)+CMB+GC+ H_0 , the SN(SALT2)+CMB+GC+ H_0 , and the SN(SiFTO)+CMB+GC+ H_0 data, respectively. The current values of $\{S_3^{(1)}, S_4^{(1)}\}$ given by the “Combined”, the “SALT2” and the “SiFTO” data are marked as a black square, a red triangle and a green diamond, respectively. To make a comparison, the fixed point $\{S_3^{(1)}, S_4^{(1)}\} = \{1, 1\}$ for the Λ CDM model is also marked as a blue round dot. The difference between two models is measured by the distance between their fixed points of today. The arrows indicate the evolution directions of the models.

ACKNOWLEDGMENTS

ML is supported by the National Natural Science Foundation of China (Grant No. 11275247, and Grant No. 11335012) and 985 grant at Sun Yat-Sen University. SW is supported by the National Natural Science Foundation of China under Grant No. 11405024 and the Fundamental Research Funds for the Central Universities under Grant No. N130305007.

REFERENCES

- Ade, P. A. R. et al. [Planck Collaboration], 2014, *Astron. Astrophys.* 571, 16
- Alcaniz, J. S.; Lima, J. A. S., 1999, *Astrophys. J.* 521, L87
- Alcaniz, J. S.; Lima, J. A. S.; Cunha, J. V., 2003, *Mon. Not. Roy. Astron. Soc.* 340 L39
- Amanullah, R. et al., 2010, *Astrophys. J.* 716, 712.
- Arabsalmani, M., & Sahni, V., 2011, *Phys. Rev. D* 83, 04350
- Astier, P. et al., 2006, *Astron. Astrophys.* 447 31
- Bennett, C. L., et al. 2013, *Astrophys. J. Suppl.* 208, 20
- Betoule, M. et al. 2014, *Astron. Astrophys.* 568, 22
- Caldwell, R. R.; Dave, R.; Steinhardt, P. J., 1998 *Phys. Rev. Lett.* 80, 1582
- Caldwell, R. R., 2002 *Phys. Lett. B* 545, 23
- Caldwell, R. R.; Kamionkowski, M.; Weinberg, N. N., 2003, *Phys. Rev. Lett.* 91, 071301
- Caldwell, R. R., & Kamionkowski, M., 2009, *Ann. Rev. Nucl. Part. Sci.* 59, 397
- Chevallier, M. & Polarski, D. 2001, *Int. J. Mod. Phys. D* 10, 213
- Chuang, C.-H., Wang Y. 2012, *Mon. Not. Roy. Astron. Soc.* 426, 226
- Chuang, C.-H., et al. 2013, arXiv:1312.4889
- Clarkson, C.; Cortes, M.; Bassett, B. A. 2007, *JCAP* 08 011
- Conley, A. et al., 2011, *Astrophys. J. Suppl.* 192, 1
- Delubac, T. et al., 2014, arXiv:1404.1801
- Dunlop, J. et al., 1996 *Nature* 381, 581
- Dunlop, J., *The Most Distant Radio Galaxies*, Kluwer, Dordrecht (1999)
- Gerke, B. F. & Efstathiou, G., 2002, *Mon. Not. Roy. Astron. Soc.* 335, 33
- Gong, Y.; Gao, Q.; Zhu Z.-H., 2013, *Mon. Not. Roy. Astron. Soc.* 430, 3142
- Huang, Q.-G.; Li, M.; Li, X.-D.; Wang, S. 2009, *Phys. Rev. D* 80, 083515
- Huterer, D. & Starkman, G. 2003, *Phys. Rev. Lett.* 90, 031301
- Huterer, D. & Cooray, A. 2005, *Phys. Rev. D* 71, 023506
- Frieman, J., Turner, M., Huterer, D., 2008 *Ann. Rev. Astron. Astrophys.* 46, 385
- Guo, Z.-K.; Ohta, N.; Tsujikawa S., 2007 *Phys. Rev. D* 76, 023508
- Guy, J. et al., 2010, *Astron. Astrophys.* 523, 7.
- Hasinger, G.; Scharrel, N.; Komossa, S., 2002, *Astrophys. J.* 573, L77
- He, J.-H.; Wang, B.; Abdalla, E.; D. Pavon, 2010, *JCAP*. 12 022
- Hicken, M. et al., 2009, *Astrophys. J.* 700 331.
- Jassal, H. K.; Bagla, J. S.; Padmanabhan, T., 2005, *Phys. Rev. D* 72, 103503

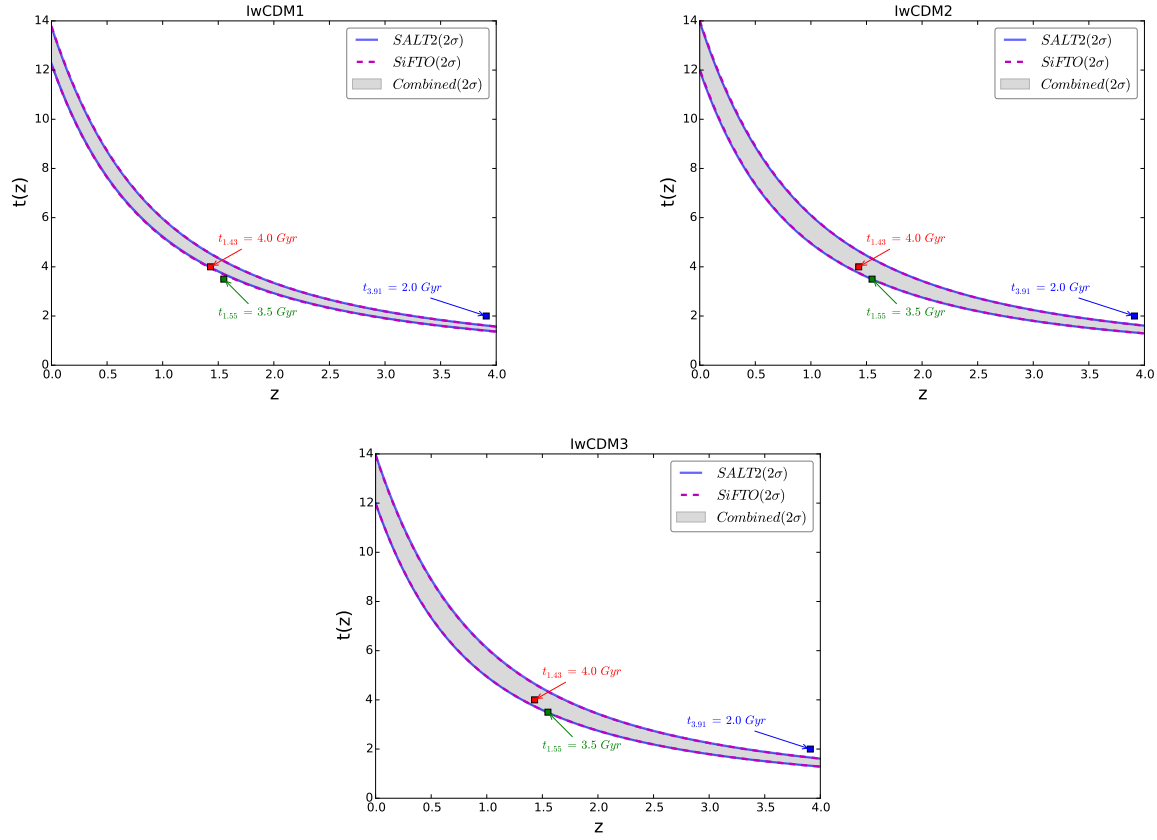


Figure 6. (color online). The 2σ confidence regions of cosmic age $t(z)$ at redshift region $[0, 4]$, for the $IwCDM1$ (upper left panel), the $IwCDM2$ (upper right panel) and the $IwCDM3$ (lower panel) model. Three $t(z)$ data points, $t_{1.43}$, $t_{1.55}$ and $t_{3.91}$, are also marked by Squares for comparison. “Combined” (gray filled regions), “SALT2” (blue solid lines), and “SiFTO” (purple dashed lines) denote the results given by the SN(Combined)+CMB+GC+ H_0 , the SN(SALT2)+CMB+GC+ H_0 , and the SN(SiFTO)+CMB+GC+ H_0 data, respectively.

Kessler, R. et al., 2009, *Astrophys. J. Suppl.* 185, 32
Kowalski, M. et al., 2008 *Astrophys. J.* 686 749
Lan, M.-X.; Li, M.; Li, X.-D.; Wang, S., 2010, *Phys. Rev. D* 82, 023516
Lewis, A. and Bridle, S., 2002, *Phys. Rev. D* 66, 103511
Li, M.; Li, X.-D.; Wang, S.; Wang, Y.; Zhang X., 2009, *JCAP* 0912, 014
Li, M.; Li, X.-D.; Wang, S.; Wang, Y., 2011, *Commun. Theor. Phys.* 56, 525
Li, X.-D et al., 2011, *JCAP* 07, 011
Li, X.-D.; Wang, S.; Huang, Q.-G.; Zhang X.; Li, M., 2012, *Sci. China Phys. Mech. Astron.* 55, 1330
Li, Y.-H.; Zhang, J. F.; Zhang, X. 2014 *Phys. Rev. D* 90, 063005
Li, Y.-H.; Zhang, X. 2014 *Phys. Rev. D* 89, 083009
Linder, E. V., 2003 *Phys. Rev. Lett.* 90, 091301
Liu, S.; Zhang, T. J., 2014, *Phys. Lett. B* 733, 69
Marriner, J. et al., 2011, *Astrophys. J.* 740, 72
Mohlabeng, G. M.; Ralston, J. P., 2013, *Mon. Not. Roy. Astron. Soc.* 439, L16
Perlmutter S. et al. 1999, *Astrophys. J.* 517, 565
Riess A. et al. 1998, *AJ* 116, 1009
Riess A. et al. 2011, *Astrophys. J.* 730, 119
Sahni, V.; Shafieloo, A.; Starobinsky, A. A., 2014, *Astrophys. J.* 793, L40
Samushia, L. et al., 2013, *MNRAS* 429, 1514
Scolnic, D. et al., 2014, *Astrophys. J.* 795, 45

Suzuki, N. et al., 2012, *Astrophys. J.* 746, 85
Uzan, J. P. 2010, *General Relativity and Gravitation*, 42, 2219
Visser, M. 2004, *Class. Quant. Grav.* 21, 2603
Wang, S.; Zhang, Y., 2008, *Phys. Lett. B* 669, 201
Wang, S.; Li, X.-D.; Li, M., 2010, *Phys. Rev. D* 82, 103006
Wang, Y., *Dark Energy*, Wiley-VCH (2010)
Wang, S.; Li, X.-D.; Li, M. 2011, *Phys. Rev. D* 83, 023010
Wang, S.; Wang, Y., 2013, *Phys. Rev. D* 88, 043511
Wang, Y.; Wang, S., 2013, *Phys. Rev. D* 88, 043522
Wang, S.; Li, Y.-H.; Zhang, X. 2014, *Phys. Rev. D* 89, 063524
Wang, S.; Wang, Y.-Z.; Geng, J.-J.; Zhang X. 2014, *Eur. Phys. J. C* 74, 3148
Wang, S.; Wang, Y.-Z.; Zhang X. 2014, *Commun. Theor. Phys.* 62, 927
Wang, S.; Geng, J.-J.; Hu, Y.-L.; Zhang X., 2015, *Sci. China Phys. Mech. Astron.* 58, 019801
Wei, H.; Zhang, S. N., 2007, *Phys. Rev. D* 76, 063003
Weinberg, D. H.; Mortonson, M. J.; Eisenstein, D.J.; Hirata, C.; Riess, A. G.; Rozo, E. 2013, *Physics Reports*, 530, 87
Wetterich, C., 2004, *Phys. Lett. B* 594, 17
Yan, X.-P.; Liu, D.-Z.; Wei, H., 2014, *arXiv:1411.6218*
Zlatev, I.; Wang, L.; Steinhardt, P. J., 1999, *Phys. Rev. Lett.* 82, 896

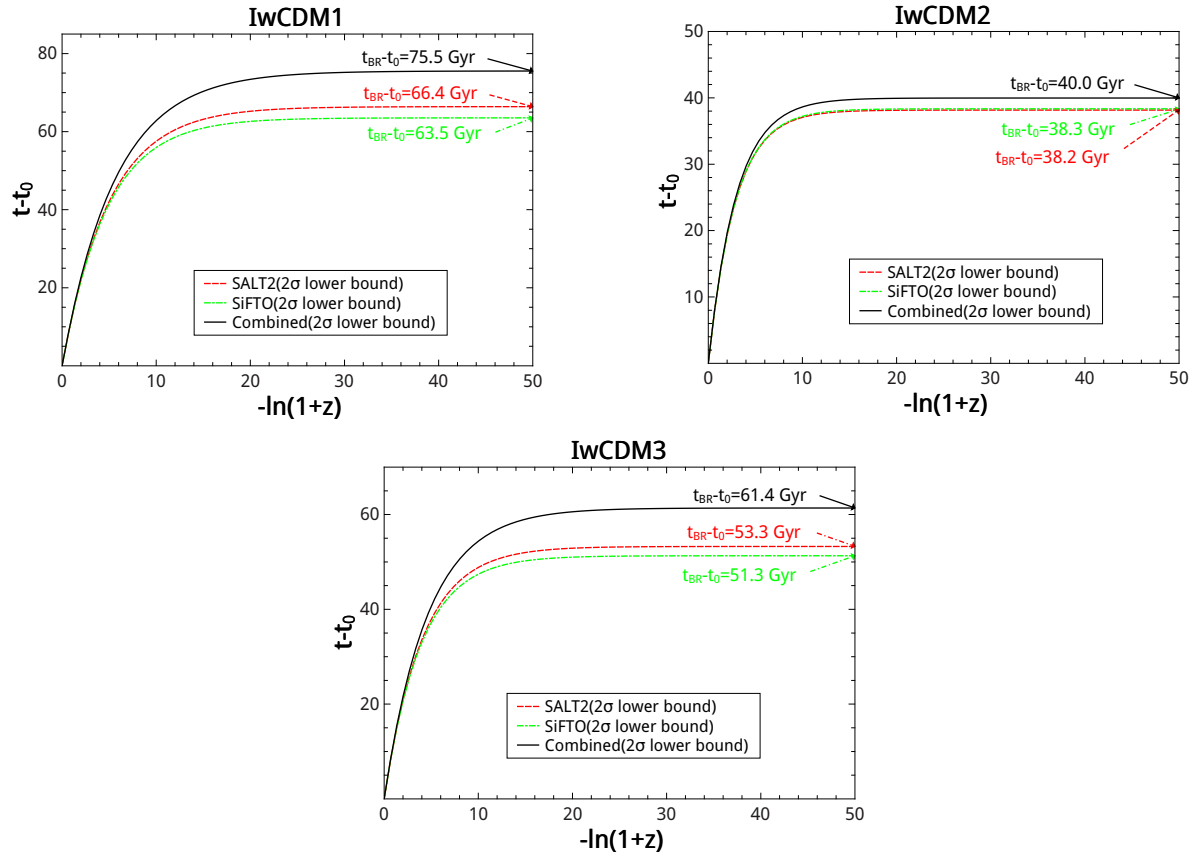


Figure 7. (color online). The 2σ lower limits of the time interval $t - t_0$ between a future moment and today, for the $IwCDM1$ (upper left panel), the $IwCDM2$ (upper right panel) and the $IwCDM3$ (lower panel) model. “Combined” (black solid lines), “SALT2” (red dashed lines), and “SiFTO” (green dash-dotted lines) denote the results given by the SN(Combined)+CMB+GC+ H_0 , the SN(SALT2)+CMB+GC+ H_0 , and the SN(SiFTO)+CMB+GC+ H_0 data, respectively. The 2σ lower bound values of $t_{BR} - t_0$ given by the three SNLS3 data are also listed on this figure.